Applied Catalysis B: Environmental 342 (2024) 123424

Contents lists available at ScienceDirect

Applied Catalysis B: Environmental

journal homepage: www.elsevier.com/locate/apcatb

Shielding ceria based catalysts from SO_2 poisoning in NH_3-SCR reaction: Modification effect of acid metal oxides

Yandi Cai [a,b,c], Bifeng Zhang [a,b,c], Haowei Yu [a,b,c], Xiaoyu Ji [a,b,c], Jingfang Sun [a,b,c], Xizhang Wang [d], Qiuhui Qian [e], Lulu Li [f], Annai Liu [g], Wei Tan [a,b,c,*], Fei Gao [a,b,c,*], Lin Dong [a,b,c]

[a] Key Laboratory of Mesoscopic Chemistry of MOE, School of Chemistry and Chemical Engineering, Nanjing University, Nanjing 210023, PR China
[b] Jiangsu Key Laboratory of Vehicle Emissions Control, Center of Modern Analysis, PR China
[c] State Key Laboratory of Pollution Control and Resource Reuse, School of Environment, School of Chemistry and Chemical Engineering, Nanjing University, Nanjing 210023, PR China
[d] Key Laboratory of Mesoscopic Chemistry of MOE and Jiangsu Provincial Laboratory for Nanotechnology, School of Chemistry and Chemical Engineering, Nanjing University, Nanjing 210023 PR China
[e] National and Local Joint Engineering Laboratory of Municipal Sewage Resource Utilization Technology, School of Environmental Science and Engineering, Suzhou University of Science and Technology, Suzhou 215009, China
[f] School of Environmental and Chemical Engineering, Jiangsu University of Science and Technology, Zhenjiang 212003, PR China
[g] Sinopec Catalyst Co. Ltd., Sinopec Group, Beijing 100029, PR China

ARTICLE INFO

Keywords:
NH_3-SCR
CeO_2
Acid metal oxides
Shielding effect
SO_2 resistance

ABSTRACT

Modifying CeO_2 with acid sites is a common strategy for designing efficient catalysts for the selective catalytic reduction of NO_x by NH_3 (NH_3-SCR of NO_x). However, the effect of acid metal oxide modification on the SO_2 resistance of CeO_2 has not been well revealed. In this work, it was found that the SO_2 resistance of CeO_2 modified with several acid metal oxides (*i.e.*, MoO_3, WO_3 and Nb_2O_5), followed an order of $Mo/CeO_2 \geq W/CeO_2 > Nb/CeO_2$. Further systematic characterizations revealed that Mo-OH and W-OH on CeO_2 as Brønsted acid sites could better inhibit the SO_2 adsorption and the sulfation of active sites than highly dispersed NbO_x mainly as Lewis acid sites because NH_4^+ coordinated to Brønsted acid sites could help trap SO_2 to form ammonium sulfates rather than metal sulfates. The findings in this work provided important guidance for the design of efficient catalysts with superior SO_2 resistance performance.

1. Introduction

Nitrous oxides (NO_x) emitted by both mobile and stationary sources have been considered one of the most dangerous air pollutants, which could result in serious air pollution problems (*e.g.*, photochemical smog, haze and acid rain, *etc.*) [1,2]. Driven by the tightening policies and increasing environmental awareness, various techniques, such as selective non-catalytic reduction of NO_x (SNCR), urea or ammonia selective catalytic reduction of NO_x (urea-SCR or NH_3-SCR), *etc.*, have been developed to realize elimination of NO_x [3–5]. Among them, NH_3-SCR of NO_x was the most efficient one , and the efficient catalyst is the core of NH_3-SCR technique [6,7]. By far, the most popular commercial catalyst for NH_3-SCR is V_2O_5-WO_3(MoO_3)/TiO_2, which exhibited superior deNO_x efficiency as well as satisfactory resistance to SO_2 poisoning at 300–400 °C [8,9]. However, the relatively poor low-temperature activity and the biological toxicity posed by vanadium have led researchers to seek an alternative catalyst with enhanced low-temperature activity and satisfactory environmental friendliness.

Recently, environmentally benign ceria (CeO_2) based catalytic materials with superior redox properties have caught the attention of researchers for their potential in NH_3-SCR of NO_x [10–14]. Since the NH_3-SCR reaction was composed of two half reactions, *i.e.*, redox cycle and acidity cycle, to enhance the NH_3-SCR performance of CeO_2 based materials, modifying CeO_2 with acid metal oxides as new acid sites for NH_3 adsorption/activation has been taken as the most effective strategy. For example, Peng *et al.* reported that CeO_2 doped with WO_3 exhibited superior NH_3-SCR activity because WO_3 species could act as acid sites to facilitate the adsorption and activation of NH_3 [15]. Similarly, $CeZrO_x$ catalysts modified with Nb_2O_5 and MoO_3 were also found to exhibit enhanced NH_3-SCR activity due to the improved surface acidity

* Corresponding authors at: Key Laboratory of Mesoscopic Chemistry of MOE, School of Chemistry and Chemical Engineering, Nanjing University, Nanjing 210023, PR China.
E-mail addresses: tanwei@nju.edu.cn (W. Tan), gaofei@nju.edu.cn (F. Gao).

https://doi.org/10.1016/j.apcatb.2023.123424
Received 28 July 2023; Received in revised form 10 October 2023; Accepted 21 October 2023
Available online 23 October 2023

[16–18]. Moreover, as reported by us previously, besides using as acid sites for NH_3 adsorption, CeO_2 based materials modified with different acid metal oxides (*e.g.*,WO_3, MoO_3 and Nb_2O_5, *etc.*) showed different adsorption properties to reactant molecules, especially NO_x [19,20]. Specifically, highly dispersed WO_3 and MoO_3 could hinder the adsorption of NO_x on CeO_2, while Nb_2O_5 deposited on CeO_2 showed much less inhibition effect on the NO_x adsorption. It was also found that CeO_2 modified with MoO_3 exhibited superior resistance to SO_2 adsorption, the first step in the SO_2 poisoning progress on NH_3-SCR catalysts [21–23], thus helping alleviate SO_2 poisoning of CeO_2. Inspired by this, it was proposed that the modification with different acid metal oxides could change the adsorption characteristics of SO_2 on CeO_2 to different degrees, then generate different SO_2 resistance performance. Since improving the SO_2 resistance of CeO_2 based catalysts has become one of the hottest topics in the practical application of CeO_2 in low temperature NH_3-SCR of NO_x and some other important reactions in the energy and environmental catalysis field, it is undoubtedly important to reveal the role of different metal oxides in shielding CeO_2 from SO_2 poisoning.

In this work, aimed at revealing the promotion effect of acid metal oxides modification on the NH_3-SCR activity and SO_2 resistance ability of CeO_2, and finding the most suitable acid metal oxide to achieve better SO_2 resistance, a series of CeO_2 catalysts modified with the optimal loadings of WO_3, MoO_3 and Nb_2O_5 were selected as model catalysts, and systematic catalytic performance/SO_2 resistance evaluation, various characterizations as well as mechanism study were conducted. It was deeply revealed that highly dispersed MoO_3 could better shield CeO_2 from SO_2 poisoning than highly dispersed WO_3 and Nb_2O_5 in NH_3-SCR reaction, which provided important guidance for the design of efficient catalysts with superior SO_2 resistance performance.

2. Materials and experimental methods

2.1. Catalyst preparation

WO_3/CeO_2, MoO_3/CeO_2 and Nb_2O_5/CeO_2 catalysts used in this work were prepared by wetness impregnation method. The CeO_2 support was prepared by thermal decomposition of $Ce(NO_3)_3{\cdot}6\ H_2O$ in air at 550 °C for 4 h, with a ramping rate of 2 °C•min^{-1}. To deposit WO_3, MoO_3 and Nb_2O_5 onto CeO_2, a certain amount of the precursors of WO_3 ($H_{40}N_{10}O_{41}W_{12}{\cdot}nH_2O$), MoO_3 ($(NH_4)_6Mo_7O_{24}{\cdot}4\ H_2O$) or Nb_2O_5 ($C_4H_4NNbO_9{\cdot}nH_2O$) and oxalic acid (molar ratio of metals in precursor to oxalic acid was 1:1.5) were first dissolved in deionized water under vigorous stirring, and then CeO_2 support was added to the solution. Afterwards, the mixture was evaporated at 110 °C under vigorous stirring. The obtained solid was dried at 110 °C for 12 h, followed by the calcination in air at 500 °C for 4 h, with a ramping rate of 2 °C•min^{-1}. The prepared WO_3/CeO_2, MoO_3/CeO_2 and Nb_2O_5/CeO_2 catalysts were denoted as xW/CeO_2, yMo/CeO_2 and zNb/CeO_2 (x, y or z mmol per 1000 m^2 CeO_2 = The loading of WO_3, MoO_3 or Nb_2O_5 on CeO_2). According to the results of further catalytic performance evaluation, WO_3/CeO_2, MoO_3/CeO_2 and Nb_2O_5/CeO_2 catalysts with optimal loadings were denoted as W/CeO_2, Mo/CeO_2 and Nb/CeO_2, respectively. For further catalytic performance evaluation, the catalysts were tableted and sieved into 40–60 mesh.

The catalysts after SO_2 resistance test were denoted as W/CeO_2-used, Mo/CeO_2-used and Nb/CeO_2-used. The catalyst after regeneration was denoted as W/CeO_2-R, Mo/CeO_2-R and Nb/CeO_2-R.

2.2. Catalytic performance evaluation

The NH_3-SCR activity and N_2 selectivity on the prepared catalysts were evaluated on a fixed-bed quartz tube reactor. For each test, 200 mg catalyst was loaded into the middle of the quartz tube. The feeding gas consisted of 500 ppm NO, 500 ppm NH_3, 5% O_2 and 100 ppm SO_2 (when used), using N_2 as balance. For all tests, the total flow rate was 200 mL•min^{-1}, giving a WHSV (weight hourly space velocity) of 60,000 mL g^{-1} h^{-1}. The effluent gas was continuously analyzed on an online Thermofisher iS10 FT-IR spectrometer equipped with a 2 m path-length gas cell (250 mL volume). The NO_x conversion and N_2 selectivity were determined according to the following equations:

$$NO_x\ \text{conversion}\ (\%) = \frac{[NO]_{in} - [NO]_{out} - [NO_2]_{out}}{[NO]_{in}} \times 100\%$$

$$N_2\ \text{selectivity}\ (\%) = \frac{[NO]_{in} - [NO]_{out} + [NH_3]_{in} - [NH_3]_{out} - [NO_2]_{out} - 2[N_2O]_{out}}{[NO]_{in} - [NO]_{out} + [NH_3]_{in} - [NH_3]_{out}} \times 100\%$$

2.3. Catalyst characterization

The specific surface area of samples was measured by N_2-physisorption at 77 K on a Micromeritics ASAP-2020 analyzer *via* Brunauer-Emmet-Teller (BET) method. Before each test, the sample was degassed in vacuum at 300 °C for 3 h.

X-ray powder diffraction (XRD) patterns were collected on a Philips X′pert Pro diffractometer (APL, Switzerland) using Ni-filtered Cu Kα radiation (λ = 0.15418 nm). The X-ray tube was operated at 40 kV and 40 mA. The 2θ range was from 10 to 80°. The scan step was set as 0.02°. The scan speed was controlled at 10°•min^{-1}.

Raman spectra were collected on a HORIBA (Japan) LabRAM Aramis Raman spectrometer equipped with an Ar^+ laser beam. The emission line was set at 532 nm, and the output power was 10 mW.

Thermogravimetry analysis-mass spectrum (TG-MS) analysis and differential thermal analysis (DTA) were conducted on Netzsch thermoanalyzer STA 449 C instrument. In each test, samples were heated from room temperature to 950 °C with a ramping rate of 10 °C·min^{-1} in N_2 flow (60 mL·min^{-1}). The trail gas was analyzed by an online mass spectrometer.

H_2-temperature-programmed reduction (H_2-TPR) experiments were performed on a quartz U-tube reactor connected to an online thermal conductivity detector (TCD). In each test, *ca.* 10 mg samples were loaded into the U-tube. 7% H_2/Ar (10 mL•min^{-1}) was used as reducing reagent. Prior to the reduction process, the sample was pretreated by N_2 flow (10 mL•min^{-1}) at 200 °C for 1 h, and then cooled to room temperature. The reduction process was measured from room temperature to 950 °C, with a ramping rate of 10 °C•min^{-1}·H_2O in the tail gas was removed by a cold trap before being passed into the TCD.

X-ray photoelectron spectroscopy (XPS) experiments were performed on a PHI 5000 Versa Probe system. Monochromatic Al Kα ($h\nu$ = 1486.6 eV) was used as the radiation of the instrument, and the acceleration power was 15 kW. The binding energies of all elements were calibrated with C 1 s at 284.6 eV.

NH_3-temperature-programmed desorption (NH_3-TPD) experiments were conducted on a fixed-bed quartz tube reactor connected with an online Thermofisher iS10 FT-IR spectrometer equipped with a 2 m path-length gas cell (250 mL volume). In each test, *ca.* 100 mg catalyst was loaded into the quartz tube, followed by pretreatment in Ar flow (100 mL•min^{-1}) at 300 °C for 30 min. Then the catalyst was saturated with NH_3 at room temperature. Afterwards, Ar flow (100 mL•min^{-1})

was switched on to remove the weakly adsorbed NH_3. Finally, the catalyst was heated linearly from room temperature to 600 °C in Ar flow (100 mL•min^{-1}) with a ramping rate of 5 °C·min^{-1}.

In situ diffuse reflectance infrared Fourier transform spectroscopy (*in situ* DRIFTS) experiments were carried out on a Nicolet Nexus 5700 FTIR spectrometer equipped with an MCT detector. In each test, *ca.* 50 mg catalyst was loaded into the DRIFTS cell, pressed and mounted. Then the catalyst was pretreated with N_2 flow at 450 °C for 1 h. The background spectra of samples at different temperatures were collected during the cooling process and automatically subtracted from the sample spectra. The feeding gas (50 mL•min^{-1}) consisted of 3000 ppm NH_3 (when used), 3000 ppm NO (when used), 5 vol% O_2 (when used) and 100 ppm SO_2 (when used), using N_2 as balance. The spectra were collected from 650 to 4000 cm^{-1}, with a spectral resolution of 4 cm^{-1} for 32 scans. The spectra were presented in the form of Kubelka-Munk.

3. Results And Discussion

3.1. Activity and SO_2 resistance of catalysts

The NH_3-SCR activity on xW/CeO_2, yMo/CeO_2 and zNb/CeO_2 was first tested and illustrated in Fig. S1. After the modification with WO_3, MoO_3 and Nb_2O_5, the NH_3-SCR activity on CeO_2 was significantly enhanced, which should be mainly resulted from the improvement of surface acidity [24–26]. xW/CeO_2, yMo/CeO_2 and zNb/CeO_2 also showed much higher N_2 selectivity than CeO_2 (Fig. S2). The optimal loadings of metal oxides for xW/CeO_2, yMo/CeO_2 and zNb/CeO_2 to achieve the best NH_3-SCR activity were 10, 14 and 18 mmol per 1000 m^2 CeO_2, respectively (Fig. 1**a**). CeO_2 catalysts modified with optimal loadings of WO_3, MoO_3 and Nb_2O_5 in the following sections were denoted as W/CeO_2, Mo/CeO_2 and Nb/CeO_2 for convenience.

Although a variety of CeO_2 based catalysts have been reported to exhibit superior NH_3-SCR activity even at low temperature (150–200 °C), the severe SO_2 poisoning effect made them far away from the practical application, especially in the low temperature range. Herein, to investigate the SO_2 resistance ability of W/CeO_2, Mo/CeO_2 and Nb/CeO_2 at low temperatures, NH_3-SCR activity on them was evaluated at 175 °C in the presence of 100 ppm SO_2. As shown in Fig. 1**b**, once SO_2 was introduced to the samples at 175 °C, the NO_x conversions on W/CeO_2, Mo/CeO_2 and Nb/CeO_2 all declined accordingly, which might be related to the poisoning of active sites by SO_2 or the coverage of catalyst surface by ammonium sulfates, such as NH_4HSO_4 and $(NH_4)_2SO_4$ [27,28]. However, it is interesting that CeO_2 modified with different acid metal oxides showed different deactivation trends. To better evaluate the rate of deactivation resulted from SO_2 poisoning, the NO_x conversion as a function of time was normalized based on the initial NO_x conversion on fresh samples (Fig. 1**c**). It was found that the deNO_x efficiency of Nb/CeO_2 decreased by 80% in 8 h, much worse than that of W/CeO_2 (55%) and Mo/CeO_2 (55%), indicating that WO_3-CeO_2 and MoO_3-CeO_2 paired sites could better survive than Nb_2O_5-CeO_2 paired sites in the presence of SO_2. The reasons for the slight increase in the NO conversion on CeO_2 at the beginning of adding SO_2 should be related to the deposition of sulfate species, which could act as Brønsted acid sites for the adsorption and activation of NH_3 [29].

Considering that the affinity of catalysts surface for SO_2 as well as the SO_2 adsorption amount could determine the SO_2 resistance performance of NH_3-SCR catalysts [21–23], SO_2 + O_2 penetration experiments were conducted, and the results were demonstrated in Fig. 1**d**. It was observed

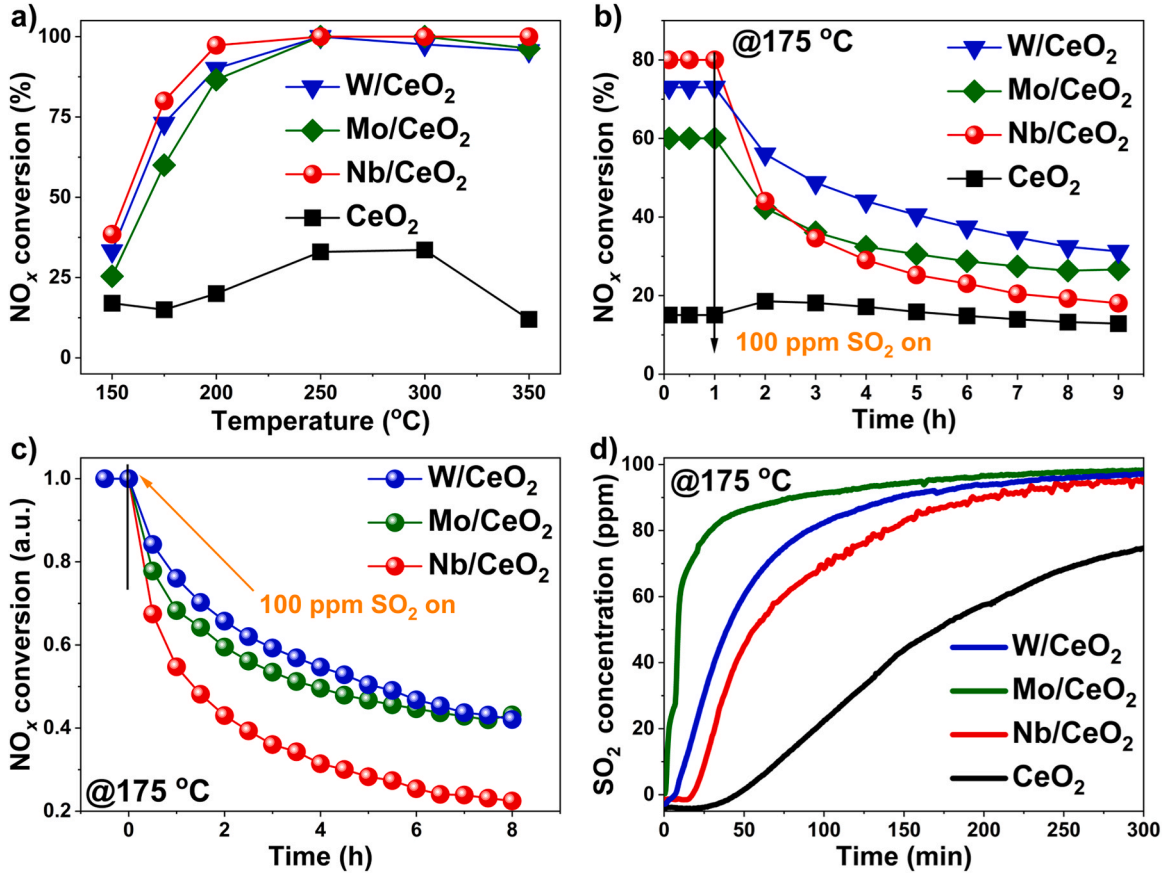

Fig. 1. a) NO_x conversions on CeO_2, W/CeO_2, Mo/CeO_2 and Nb/CeO_2 catalysts in NH_3-SCR reaction; **b)** NO_x conversions on CeO_2, W/CeO_2, Mo/CeO_2 and Nb/CeO_2 catalysts in the presence of 100 ppm SO_2 at 175 °C; **c)** Normalized NO_x conversions on W/CeO_2, Mo/CeO_2 and Nb/CeO_2 catalysts; **d)** SO_2 concentration in the outlet gas during the 100 ppm SO_2 + 5% O_2 penetration experiments at 175 °C. Reaction condition: 500 ppm NH_3, 500 ppm NO, 5% O_2, 100 ppm SO_2 (when used), Ar as balance.

that acid metal oxides loaded on CeO_2 could alleviate the adsorption of SO_2. Furthermore, Mo/CeO_2 and W/CeO_2 could be saturated with SO_2 much faster than Nb/CeO_2, indicating that MoO_3 or WO_3 could better inhibit the adsorption of SO_2 on CeO_2 than Nb_2O_5, which provided meaningful guidance for developing efficient CeO_2 based catalysts with better SO_2 resistance.

3.2. Structure of the catalysts

To better reveal the reasons for different SO_2 resistance performance of W/CeO_2, Mo/CeO_2 and Nb/CeO_2, systematic characterizations were conducted to investigate their structures. XRD patterns for CeO_2, xW/CeO_2, yMo/CeO_2 and zNb/CeO_2 were first collected (Fig. S3). For all CeO_2 catalysts modified with optimal loadings of acid metal oxides, all diffraction peaks were assigned to cubic fluorite CeO_2 (JCPDS 34–0394), and no additional peak assigned to crystalline acid metal oxides was observed, indicating that W, Mo and Nb species were highly dispersed on CeO_2.

According to the results of N_2-physisorption experiments, W/CeO_2, Mo/CeO_2 and Nb/CeO_2 showed comparable specific surface area (SSA) and pore volume (Table S1), suggesting that SSA and pore volume would not contribute to the difference in their SO_2 resistance performance. The slight decrease ($< 10\ m^2 \bullet g^{-1}$) in the SSA of CeO_2 after the deposition of acid metal oxides should be mainly due to the further calcination at 500 °C for 4 h and slight pore blocking. Moreover, after the SO_2 resistance test, almost no change was observed in the SSA of W/CeO_2, Mo/CeO_2 and Nb/CeO_2, indicating good structure stability in the presence of SO_2.

To further study the surface structure of the prepared catalysts, Raman spectra of xW/CeO_2, yMo/CeO_2 and zNb/CeO_2 were collected. For all samples, an intensive band at *ca.* 465 cm^{-1} and a broad band at *ca.* 600 cm^{-1} were observed (Fig. 2**a** and Fig. S4), which were related to the F_{2g} vibration mode of CeO_2 and oxygen defects (D band), respectively [30,31]. After the deposition of WO_3 onto CeO_2, two bands at 808 and 975 cm^{-1} emerged as the loadings increased, which could be assigned to W-O-Ce stretching vibrations and surface dispersed WO_3 species (Fig. S4a) [32–34]. When the WO_3 loadings further increase to 12 mmol per 1000 m^2 CeO_2, several bands assigned to crystalline WO_3 (274, 330, 718 cm^{-1}) were observed, matching well with the results of XRD (Fig. S3b). For yMo/CeO_2 catalysts (Fig. S4c), several bands at 700–1000 cm^{-1} could be clearly observed, which were attributed to the stretching vibration of Mo-O-X (X = Mo or Ce) and the surface molybdena species, according to the previous report [20,24,35]. With the increase of MoO_3 loading amount, a new band at 959 cm^{-1} emerged gradually and the band at 922 cm^{-1} disappeared, which was related to the formation of surface polymeric molybdena species [36]. Bands assigned to bulk MoO_3 were not observed on all yMo/CeO_2 catalysts, which was consistent with the result of XRD. In Fig. S4e, a broad band ranging from 750 to 950 cm^{-1} was observed on zNb/CeO_2, which was mainly related to polymeric niobium oxides species composed of moderately distorted octahedral [NbO_6] structures with terminal Nb═O bonds (864 cm^{-1}) [25,37,38]. In short summary, for WO_3/CeO_2, MoO_3/CeO_2 and Nb_2O_5/CeO_2 catalysts with optimal loadings, the acid metal oxides on CeO_2 were mainly in the form of highly dispersed polymeric metal oxides. Based on the results of Raman spectra (Fig. 2**a**) and previous reports [15,39,40], the configurations WO_3, MoO_3 and Nb_2O_5 species on W/CeO_2, Mo/CeO_2 and Nb/CeO_2 were proposed and demonstrated in Fig. 2**b**.

Moreover, the strong interaction between these highly dispersed acidic metal oxides and CeO_2 support might also contribute to the formation of more surface oxygen vacancies, which was further supported by the calculated relative concentration of oxygen vacancies on CeO_2, W/CeO_2, Mo/CeO_2 and Nb/CeO_2 catalysts according to their Raman spectra (Table S1, Relative concentration of oxygen defects = I_D/I_{F2g}. I_D and I_{F2g} represented the peak area of D bands and CeO_2 F_{2g} bands, respectively). The formation of more surface oxygen vacancies could better facilitate the activation of reactants, which could also account for the significantly improved catalytic performance of CeO_2 after the modification with acid metal oxides.

3.3. Sulfate species formed on CeO_2, W/CeO_2, Mo/CeO_2 and Nb/CeO_2

It has been reported that H_2-TPR technique could be used not only to explore the reducibility of the catalysts but also to investigate the sulfate species formed on catalysts after SO_2 resistance test. As shown in Fig. 3**a**, three H_2-consumption peaks were observed on the H_2-TPR profiles for CeO_2. Peak α (*ca.* 420 °C), peak β (*ca.* 540 °C) and peak γ (*ca.* 770 °C) could be attributed to the reduction of surface chemisorbed oxygen

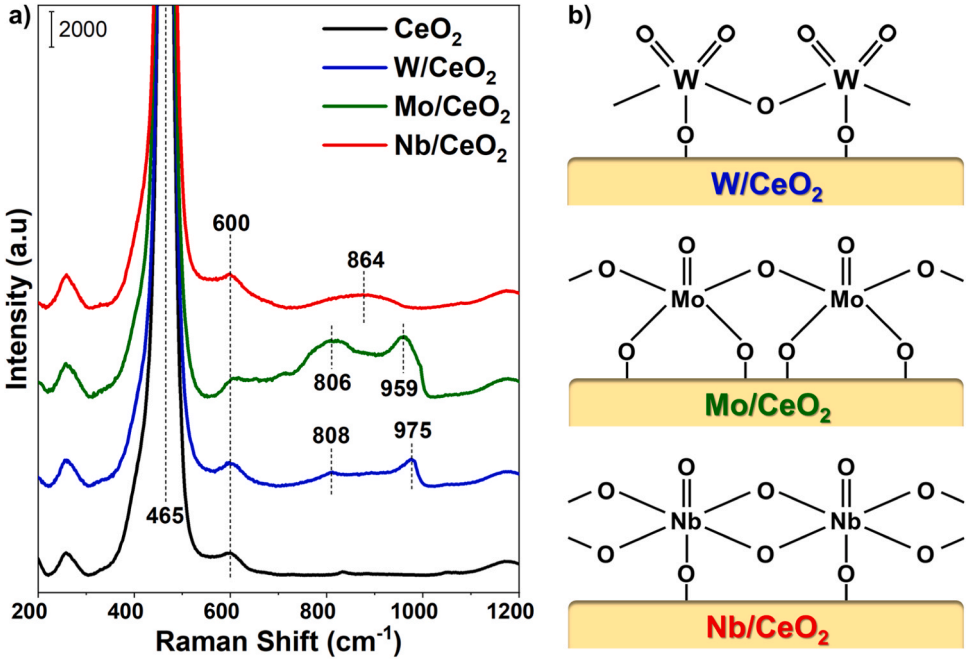

Fig. 2. a) Raman spectra for CeO_2, W/CeO_2, Mo/CeO_2 and Nb/CeO_2 catalysts. **b)** Proposed configurations of WO_3, MoO_3 and Nb_2O_5 species on CeO_2.

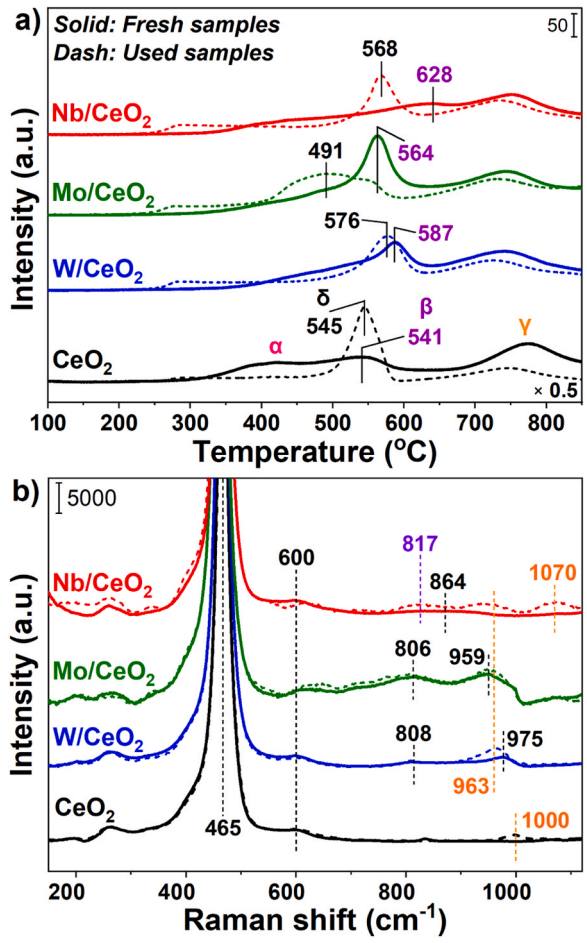

Fig. 3. **a)** H_2-TPR profiles and **b)** Raman spectra for fresh and used CeO_2, W/CeO_2, Mo/CeO_2 and Nb/CeO_2 (Solid line: fresh samples, dash line: used samples).

species, surface Ce^{4+} and bulk CeO_2, respectively [41]. After the deposition of WO_3, MoO_3 and Nb_2O_5, peak β on W/CeO_2, Mo/CeO_2 and Nb/CeO_2 were all found to shift to higher temperatures, hinting at the formation of stronger interaction between highly dispersed acid metal oxides and CeO_2 [19,42]. As discussed above, highly dispersed acid metal oxides on CeO_2 all helped generate superior NH_3-SCR activity, however, W/CeO_2, Mo/CeO_2 and Nb/CeO_2 exhibited different SO_2 resistance performance due to their different adsorption properties for SO_2. Different from the H_2-TPR profiles for fresh samples, a new H_2-consumption peak at 490–580 °C (peak δ) was observed on the H_2-TPR profiles for all used samples, which could be assigned to the reduction of the deposited sulfate species. More interestingly, the reduction of sulfate species on Mo/CeO_2 occurred at much lower temperatures than those on CeO_2-used, W/CeO_2-used and Nb/CeO_2-used, indicating that highly dispersed MoO_3 species strongly interacting with CeO_2 support could better weaken the interaction between sulfate species (SO_4^{2-}) and CeO_2 and inhibit the deep sulfation to form bulk sulfate species, thus significantly reducing the adsorption of SO_2 during the SO_2 resistance test [43,44].

To further investigate the impact of sulfate species on the states of dispersed acid metal oxides on W/CeO_2, Mo/CeO_2 and Nb/CeO_2, Raman spectra for those used catalysts were also collected (Fig. 3**b**). For CeO_2-used, a distinct peak at *ca.* 1000 cm^{-1} assigned to surface sulfate species was observed. Similarly, for W/CeO_2, Mo/CeO_2 and Nb/CeO_2, the emerged band at *ca.* 963 and 1070 cm^{-1} could also be attributed to the formation of sulfate species [45,46]. The almost negligible intensity of this band on Mo/CeO_2 further supported the viewpoint that much less sulfate species were formed on Mo/CeO_2 comparing to W/CeO_2 and Nb/CeO_2. Moreover, a new band at *ca.* 817 cm^{-1} related to the Nb-O symmetric modes of the NbO_4 tetrahedral structure was observed on Nb/CeO_2-used, suggesting that SO_2 could also react with octahedral [NbO_6] structure with terminal Nb═O bonds (864 cm^{-1}) to form NbO_4 tetrahedral structure.[47,48] The evolution of the surface structure of Nb/CeO_2 when exposed to SO_2-containing reaction flow could be one of the main reasons for its relatively poorer SO_2 resistance. As reported previously[19,49], Nb_2O_5 showed relatively better redox performance than MoO_3 and WO_3, well explaining that SO_2 could better react with Nb species on Nb/CeO_2 at a low temperature of 175 °C.

Based on the concentration of SO_2 in the outlet gas of $SO_2 + O_2$ adsorption experiment (Fig. 1**d**), it was proposed that the SO_2 adsorption capacity followed an order of Mo/CeO_2 < W/CeO_2 < Nb/CeO_2 < CeO_2. To further determine the amount of the sulfate species deposited on the catalysts after the SO_2 resistance test (Fig. 3**a**), TG-MS experiments were conducted. As shown in Fig. 4**a-d**, for all used catalysts, three weight loss steps were observed. According to previous reports, those three weight loss steps from low temperature to high temperature should be related to the desorption of adsorbed H_2O/NH_3, the decomposition of ammonium bisulfate (ABS, $2NH_4HSO_4 \rightarrow 2NH_3 + 2\,H_2O + 2SO_2 + O_2$) and the decomposition of $Ce(SO_4)_2$ or $Ce_2(SO_4)_3$ ($Ce(SO_4)_2 \rightarrow CeO_2 + 2SO_2 + O_2$, $Ce_2(SO_4)_3 \rightarrow 2CeO_2 + 3SO_2 + O_2$), respectively [46,50,51]. Interestingly, although the second step (300–550 °C) could be assigned to the decomposition of ABS, almost no SO_2 was detected in this range, which could be due to the re-adsorption of SO_2 by CeO_2 to generate extra sulfated CeO_2 species [29]. Based on this understanding, the weight loss during the third step could be used to compare the amount of sulfate species on the used catalysts.

As marked in Fig. 4, sulfate species on Mo/CeO_2-used (0.72%) were much less than those on W/CeO_2-used (1.27%) and Nb/CeO_2-used (1.50%), matching well with the expectation. The much more sulfate species on CeO_2-used (2.56%) further confirmed that highly dispersed acid metal oxides could efficiently shield CeO_2 from SO_2 poisoning, and highly dispersed MoO_3 species performed the best. Moreover, the amount of ABS formed on Mo/CeO_2 (0.50%) was higher than that on W/CeO_2-used (0.40%) and Nb/CeO_2-used (0.26%), suggesting that the total amount of sulfate species deposited on Mo/CeO_2-used is not only minimal, but also more in the form of ABS. Furthermore, it was observed that the SO_2-desorption peak on used Mo/CeO_2 was located at lower temperatures (714 °C) comparing to that on used W/CeO_2 (755 °C) and used Nb/CeO_2 (746 °C), suggesting that sulfated CeO_2 on used Mo/CeO_2 would decompose at lower temperature. Considering that the decomposition temperature (> 600 °C) of sulfated CeO_2 on all catalysts was much higher than the operation temperature of NH_3-SCR catalysts (< 500 °C), the lower desorption temperature of SO_2 on the used catalysts could not contribute to the better SO_2 resistance of Mo/CeO_2. However, the lower desorption temperature of SO_2 on Mo/CeO_2 suggested that Mo coordinated to Ce could weaken the interaction between CeO_2 and SO_2, thus inhibiting the adsorption of SO_2 on Ce sites. That is, the deep sulfation of metal sites (mainly Ce sites) on Mo/CeO_2 could be effectively retarded due to the easier reaction between NH_3 species adsorbed on Mo (Mo-O-NH_4) and SO_2 to generate ABS and inhibitory effect of Mo on the interaction between CeO_2 and SO_2.

ATR-FTIR experiments were performed to further determine the states of sulfate species on used catalysts. As shown in Fig. 5**a**, several bands assigned to various sulfate species were observed at 1626, 1165, 1127, 1108, 1055, 985, 952 and 894 cm^{-1} were related to surface sulfate species and the bands at 1211 and 985 cm^{-1} could be further assigned to the bulk sulfate species. The relatively lower intensity of these bands assigned to bulk sulfate species on Mo/CeO_2-used confirmed that Mo modification could better shield CeO_2 from deep sulfation. The bands at 952 and 894 cm^{-1} not observed on CeO_2 could be related to SO_2^{4-} species adjacent to W, Mo or Nb sites. The intensive band at *ca.* 1429 cm^{-1} could be attributed to NH_4^+ in ABS, well supporting the viewpoint that abundant ABS was deposited on the catalysts in SO_2

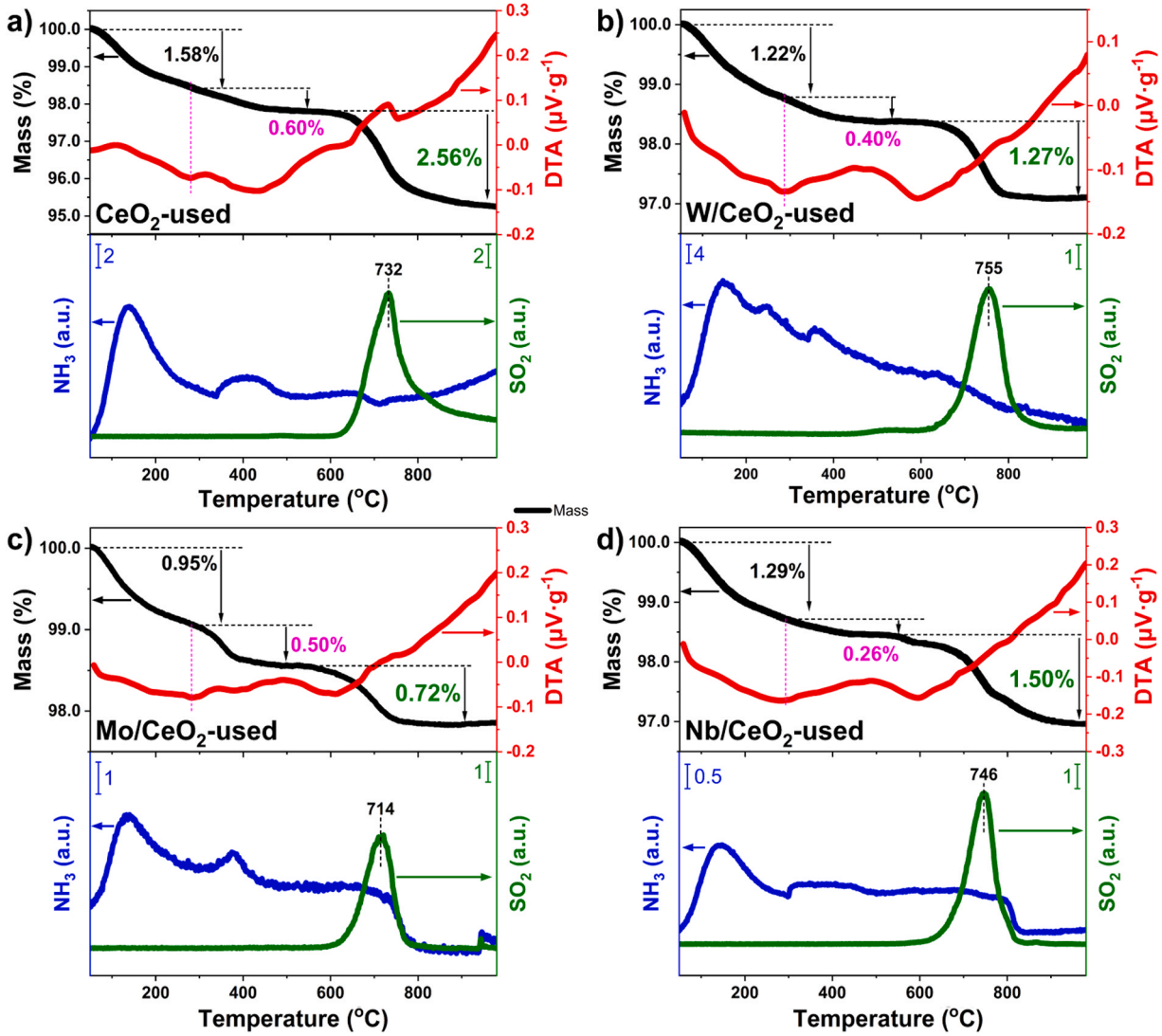

Fig. 4. TG-MS and DTA plots for **a)** CeO_2-used, **b)** W/CeO_2-used, **c)** Mo/CeO_2-used and **d)** Nb/CeO_2-used catalysts.

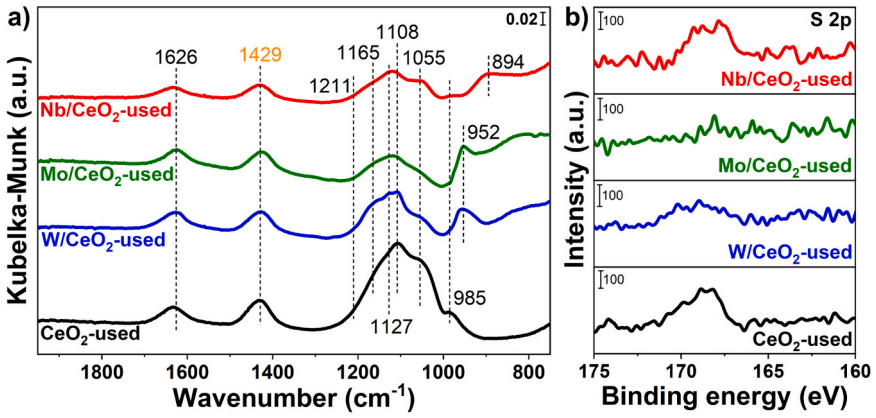

Fig. 5. **a)** ATR-FTIR spectra and **b)** S 2p XPS for used catalysts.

resistance test.

XPS experiments were conducted to further investigate the surface states as well as the amount of sulfur species on the used catalysts. As shown in Fig. 5**b**, the intensity of S 2p XPS followed an order of CeO_2 > Nb/CeO_2 > W/CeO_2 > Mo/CeO_2, in good consistence with the results of TG-MS that the least number of sulfate species were deposited on Mo/CeO_2 in the SO_2 resistance test. The relative concentration of S element on different catalysts was also calculated and listed in Table 1. XPS for W 4 f, Mo 3d and Nb 3d of fresh and used catalysts were also collected. As shown in Fig. S5a, the two peaks at *ca.* 37.3 eV (W 4 $f_{5/2}$) and *ca.* 35.2 eV

Table 1
Surface element concentration and Chemical states determined by XPS.

Samples	Surface atomic concentration (%)				Ce^{3+}/Total Ce (%)	O_α/Total O (%)
	W/Mo/Nb	Ce	O	S		
CeO_2	-	22.2	77.8	-	16.0	36.6
W/CeO_2	4.5	19.3	75.2	-	17.6	26.9
Mo/CeO_2	6.5	16.6	76.9	-	16.3	24.4
Nb/CeO_2	7.9	13.8	78.3	-	16.4	37.6
CeO_2-used	-	22.2	73.6	4.2	19.4	51.7
W/CeO_2-used	4.9	18.8	73.8	2.5	21.8	31.4
Mo/CeO_2-used	5.6	16.3	77.1	1.0	18.1	25.6
Nb/CeO_2-used	8.9	16.2	71.4	3.5	18.9	47.4

(W 4 $f_{7/2}$) on W/CeO_2 could be assigned to the W^{6+} species. Similarly, the peaks observed on Mo 3d XPS for Mo/CeO_2 and Nb 3d XPS for Nb/CeO_2 could be assigned to Mo^{6+} and Nb^{5+} species, respectively [19,20]. After being used in the SO_2 resistance test, no significant change was observed on those peaks for W/CeO_2, Mo/CeO_2 and Nb/CeO_2, indicating that SO_2 and the deposited sulfate species had limited impact on the states of W, Mo or Nb species. Moreover, the surface concentration of W, Mo and Nb species showed no significant change after the SO_2 resistance (Table 1), indicating that the dispersion of these species didn't change significantly.

Ce 3d XPS for fresh and used catalysts were also collected and further analyzed to investigate the chemical states of Ce species (Fig. S6). After the modification with WO_3, MoO_3 and Nb_2O_5, the concentration of surface Ce^{3+} on CeO_2 increased slightly, which should be due to the strong interaction between W/Mo/Nb and CeO_2 and the resulting distortion of the CeO_2 surface lattice. The formation of more Ce^{3+} on modified CeO_2 also matched well with the results of Raman spectra that more surface oxygen vacancies were formed on CeO_2 after the modification with acid metal oxides, since the formation of Ce^{3+} was always accompanied by the generation of oxygen vacancies [52]. It was also found that more Ce^{3+} species were formed on all used catalysts comparing to fresh catalysts (Fig. S7a and Table 1). As reported previously, the generation of more Ce^{3+} species in SO_2-containing atmosphere was related to the reaction between SO_2 and CeO_2 ($2CeO_2 + 3SO_2 + O_2 \rightarrow Ce_2(SO_4)_3$) [53].

O 1 s XPS for fresh and used catalysts were shown in Fig. S8. Peak O_α (*ca.* 531.8 eV) and peak O_β (*ca.* 529.6 eV) could be attributed to the surface oxygen species and lattice oxygen species, respectively [54]. As listed in Table 1, more surface oxygen species were formed on used catalysts, which should be related to the sulfated species (ABS and sulfated CeO_2). Moreover, as demonstrated by Fig. S7b, the increase in the concentration of surface oxygen species on Mo/CeO_2 (from 24.4% to 25.6%) after the SO_2 resistance test was much lower than that on CeO_2 (from 36.6% to 51.7%), W/CeO_2 (from 26.9% to 31.4%) and Nb/CeO_2 (from 37.6% to 47.4%), also confirming the formation of less sulfate species on Mo/CeO_2.

3.4. Relationship between surface acidity and deposited metal oxides/sulfate species

Considering that the surface acidity of catalysts played an important role in NH_3-SCR reaction, NH_3-TPD experiments were conducted on fresh and used catalysts (Fig. 6**a and b**). For fresh CeO_2, two NH_3-desorption peaks were observed, which were marked in red (*ca.* 160 °C, peak α) and blue (*ca.* 242 °C, peak β). Peak α and peak β could be assigned to the desorption of NH_3 bound to acid sites with weak and medium strength, respectively [44,55]. After being modified with W, Mo or Nb, an additional intensive NH_3-desorption peak marked in green was observed at higher temperatures (*ca.* 300 °C, peak γ), which should be related to the highly dispersed WO_3, MoO_3 and Nb_2O_5 species serving as Brønsted acid sites or Lewis acid sites with strong strength. The improvement of surface acidity could be one of the main reasons for the enhanced NH_3-SCR activity on CeO_2 modified with WO_3, MoO_3 and Nb_2O_5.

After the SO_2 resistance test, the total amount of desorbed NH_3 on used catalysts was much higher than that on fresh catalysts. As reported previously, the increase in the total amount of acid sites on sulfated catalysts could be due to the deposition of abundant sulfate species, which could act as Brønsted acid sites [56]. For used CeO_2, the presence of peak γ well supported the viewpoint that sulfated species deposited on CeO_2 could significantly enhance the surface acid species. However, NH_3 species (mainly in the form of NH_4^+) linked to sulfate species showed poor activity at low temperatures (≤ 175 °C). In addition, the increase in the amount of acid sites on different catalysts followed an order of CeO_2 (113 μmol·g^{-1}) > Nb/CeO_2 (83 μmol·g^{-1}) > W/CeO_2 (71 μmol·g^{-1}) > Mo/CeO_2 (43 μmol·g^{-1}), which was also highly correlated to the amount of sulfate species deposited on these catalysts.

To further determine the type of acid sites on fresh and used catalysts, *in situ* DRIFTS of NH_3 adsorption experiments were conducted (Fig. 6**c-j**). Generally speaking, the peaks at 1100–1250 cm^{-1} and 1580–1600 cm^{-1} were mainly related to the NH_3 coordinated to Lewis acid sites (NH_3-L), while the peak at 1400–1500 cm^{-1} and 1650–1800 cm^{-1} could be attributed to NH_4^+ species linked to Brønsted acid sites (NH_3-B). Other distinct bands should be ascribed to various nitrate species (Nit) generated by the oxidation of NH_3 species. For fresh CeO_2, NH_3 species were mainly adsorbed on Lewis acid sites, and NH_3-L species desorbed vigorously at low temperatures (< 200 °C), matching well with the results of NH_3-TPD (Fig. 6**a**). After the SO_2 resistance test, IR bands assigned to NH_3-L species were not observed at low temperatures, which should be related to the sulfation of surface CeO_2. The more intensive bands at *ca.* 1430 and 1680 cm^{-1} observed on CeO_2-used should be related to NH_3 species adsorbed on sulfated CeO_2 (Brønsted acid sites). A new band at *ca.* 1300 cm^{-1} assigned to NH_3 coordinated to Lewis acid sites was observed when the temperature increased to 200 °C or higher, due to the migration of NH_3 species from Brønsted acid sites to Lewis acid sites [57,58]. Different from what was observed on CeO_2, for fresh W/CeO_2 and Mo/CeO_2 catalysts, much more Brønsted acid sites were formed, and relatively weaker NH_3-L bands were observed on both W/CeO_2 and Mo/CeO_2 catalysts, suggesting that highly dispersed WO_3 and MoO_3 species on CeO_2 would mainly act as Brønsted acid sites. More interestingly, although intensive NH_3-B bands still could be observed on W/CeO_2-used and Mo/CeO_2-used, the intensity of NH_3-L bands on used catalysts was much weaker than that on fresh catalysts (Fig. 6**e-h**), which could be resulted from the sulfation of Lewis acid sites. Intensive NH_3-L and NH_3-B bands could be observed on fresh Nb/CeO_2 catalyst, which meant that highly dispersed NbO_x sites on CeO_2 could serve as both Lewis acid sites and Brønsted acid sites showing higher acid strength than those on bare CeO_2 (Fig. 6**i**). After the SO_2 resistance test, more Brønsted acid sites were formed on Nb/CeO_2 and the intensity of NH_3-L bands showed a sharp decrease simultaneously (Fig. 6**j**), indicating that both Nb and Ce sites were sulfated or covered by ammonium sulfates. In short summary, W/Mo/Nb modification could greatly enhance the surface acidity of CeO_2 from the aspect of amount and strength. After exposure to the SO_2-containing reaction stream, the surface sulfation of the catalysts would lead to an increase in Brønsted acid sites and a significant loss of Lewis acid sites.

According to the results of Raman spectra, TG-MS, ATR-FTIR, XPS and (*in situ*) NH_3-TPD experiments, the surface states of the used catalysts could be proposed. As shown in Fig. 7**a**, after the SO_2 resistance test, abundant surface sulfate species (ceric sulfates and ammonium sulfate species) were formed. After being modified with acid metal oxides, the amount of sulfate species deposited on CeO_2 decreased to different degrees, due to their shielding effect. For W/CeO_2 and Mo/CeO_2 catalysts (Fig. 7**b and c**), surface Brønsted acid sites (W-OH or Mo-

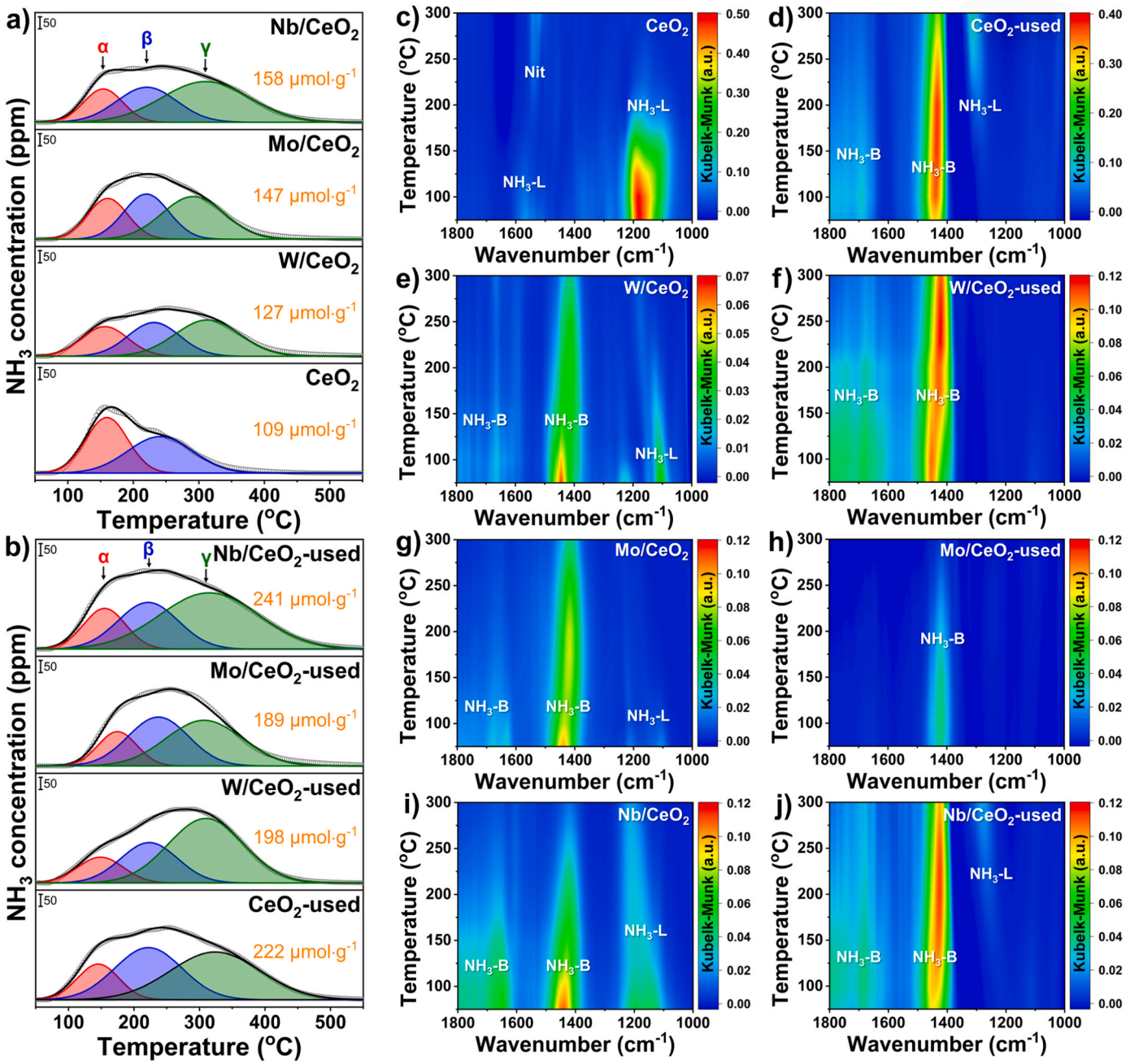

Fig. 6. NH_3-TPD profiles for **a)** fresh and **b)** used catalysts. *In situ* DRIFT of NH_3-TPD on **c)** CeO_2, **d)** CeO_2-used, **e)** W/CeO_2, **f)** W/CeO_2-used, **g)** Mo/CeO_2, **h)** Mo/CeO_2-used, **i)** Nb/CeO_2 and **j)** Nb/CeO_2-used catalysts.

OH) could trap SO_x *via* generating ammonium sulfate species, and thus inhibit the direct interaction between SO_2 and CeO_2. Moreover, polymeric tungsten/molybdenum oxides were stable when exposed to SO_2-containing atmosphere, and Ce coordinated with Mo showed lower reactivity with SO_2, as confirmed by the $SO_2 + O_2$ adsorption experiments (Fig. 1**d**). In contrast, for Nb/CeO_2 (Fig. 7**d**), fewer surface Brønsted acid sites and the reaction between polymeric niobium oxides and SO_2 would result in the deposition of more sulfate species, which accounted for the weaker SO_2 resistance of Nb/CeO_2 comparing to W/CeO_2 and Mo/CeO_2. The lower adsorption of SO_2 on Mo/CeO_2 in NH_3-SCR reaction should be attributed to the lower reactivity of Ce coordinated with Mo (Mo-O-Ce) to SO_2 and inhibitory effect of Mo-OH on the direct interaction between SO_2 and Ce by trapping SO_2 to form ABS.

3.5. Reaction mechanism

In situ DRIFTS of $NO + O_2$ reacting with pre-adsorbed NH_3, and NH_3 reacting with pre-adsorbed NO_x species were conducted at a relatively low temperature of 175 °C to determine the active sites and reveal the reaction mechanism. Since Mo/CeO_2 and W/CeO_2 showed similar surface adsorption properties (Fig. 6), to simplify the workload, Mo/CeO_2, and Nb/CeO_2 were selected as the research objects. As shown in Fig. 8**a**, after the introduction of $NO + O_2$ flow to Mo/CeO_2 pre-adsorbed with NH_3, the intensity of the bands assigned to NH_3-L species (1183 and 1229 cm^{-1}) decreased rapidly and these two peaks vanished in 5 min, while NH_3-B species (1420 cm^{-1}) showed relatively lower reactivity to $NO + O_2$, indicating that NH_3-L species were more reactive than NH_3-B [59,60]. The consumption of NH_3 could also be well demonstrated by the change of IR bands at 2500–3500 cm^{-1}, ascribed to the adsorbed

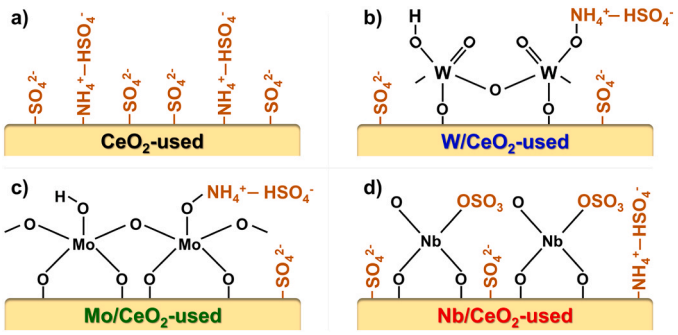

Fig. 7. Proposed surface states of **a)** CeO_2-used, **b)** W/CeO_2-used, **c)** Mo/CeO_2-used and **d)** Nb/CeO_2-used catalysts. For simplicity, all ammonium species were presented in the form of ammonium bisulfates.

NH_3 species as well [56]. It was interesting to see that almost no adsorbed NO_x species were formed on Mo/CeO_2 in 30 min, suggesting that the highly dispersed MoO_x species could effectively inhibit the adsorption of NO_x, and the NH_3-SCR reaction on Mo/CeO_2 mainly followed Eley-Rideal (E-R) mechanism. For Nb/CeO_2, both NH_3-L species (1126 and 1210 cm^{-1}) and NH_3-B species (1420 cm^{-1}) showed superior reactivity in NO + O_2 flow, which were all consumed in 6 min (Fig. 8**b**). That's why Nb/CeO_2 showed slightly higher NH_3-SCR activity than Mo/CeO_2 at low temperature. When Nb/CeO_2 was saturated with NO_x, NO + O_2 flow was switched off and Nb/CeO_2 was purged by N_2 flow to remove weakly adsorbed NO_x. Afterwards, NH_3 flow was introduced to the DRIFTS cell again to investigate the reactivity of NO_x-ad species. Although the intensity of the band attributed to chelating bidentate nitrate species (1571 cm^{-1}) decreased slightly with the introduction of NH_3, the band related to bridging bidentate nitrate species (1594 cm^{-1}) was enhanced simultaneously, indicating that the adsorbed nitrate species on Nb/CeO_2 would undergo a transformation instead of consumption when exposed to NH_3 [61–63]. So, the NH_3-SCR reaction on both Mo/CeO_2 and Nb/CeO_2 catalysts was proceeded by E-R mechanism.

To further understand the evolution of surface states of the catalysts in the presence of SO_2, *in situ* DRIFTS of NH_3-SCR + SO_2 experiments were performed (Fig. 9). For Mo/CeO_2, NH_3-L and NH_3-B species were observed when exposed to NH_3-SCR flow, and no identifiable bands related to nitrate species could be found, further suggesting that the adsorption of NO_x on Mo/CeO_2 was inhibited. Upon the introduction of SO_2 to the feeding gas, a broad band centered at 1122 cm^{-1} emerged on Mo/CeO_2, which was attributed to sulfate species and enhanced with reaction time [29,44]. Moreover, it was found that the intensity of bands attributed to NH_3-B species increased with the introduction of SO_2, which could be due to the formation of sulfated species serving as Bronsted acid sites, matching well with the results of NH_3-TPD. The enhancement in the bands related to NH_3-B species also occurred on Nb/CeO_2 when exposed to NH_3-SCR + SO_2 flow. Although the overlap of bands assigned to sulfates species and NH_3-L made it difficult to directly observe the interaction between SO_2 and Lewis acid site, *in situ* DRIFTS of NH_3-TPD results well proved that SO_2 would react with Lewis acid sites and then result in the vanishment of Lewis acid sites. Remarkably, different from what was observed on Mo/CeO_2, multiple IR bands attributed to sulfated species (1007, 1025, 1091, 1126, 1154, 1240, 1270 and 1294 cm^{-1}) were observed on Nb/CeO_2 [29,44], which could be due to that SO_2 could interact with both Nb and Ce sites as discussed in Raman spectra section (Fig. 3**b**).

As illustrated in Fig. 10, the reactivity of adsorbed NH_3 species on sulfated catalysts (after the test shown in Fig. 9) were also evaluated. NH_3-B species on sulfated Mo/CeO_2 were found to be still reactive to NO + O_2 flow, however, it would take *ca.* 30 min to complete the consumption of NH_3 (Fig. 10**a**), confirming that SO_2 would result in the deactivation of Mo/CeO_2. As for Nb/CeO_2, the surface sulfation also led to the decrease in the reactivity of adsorbed NH_3 species, and NH_3-B species on sulfated Nb/CeO_2 even showed lower reactivity than those on sulfated Mo/CeO_2, in good consistence with the results of SO_2 resistance test (Fig. 1**b**). It should also be noted that the change in the intensity of IR bands assigned to various sulfate species on Nb/CeO_2 could be due to the consumption of NH_3 adsorbed on sulfated species linked to Nb sites. Since no band attributed to nitrate species emerged throughout the test, it could be concluded that the NH_3-SCR reaction on Mo/CeO_2 and W/CeO_2 followed E-R mechanism before and after sulfation treatment.

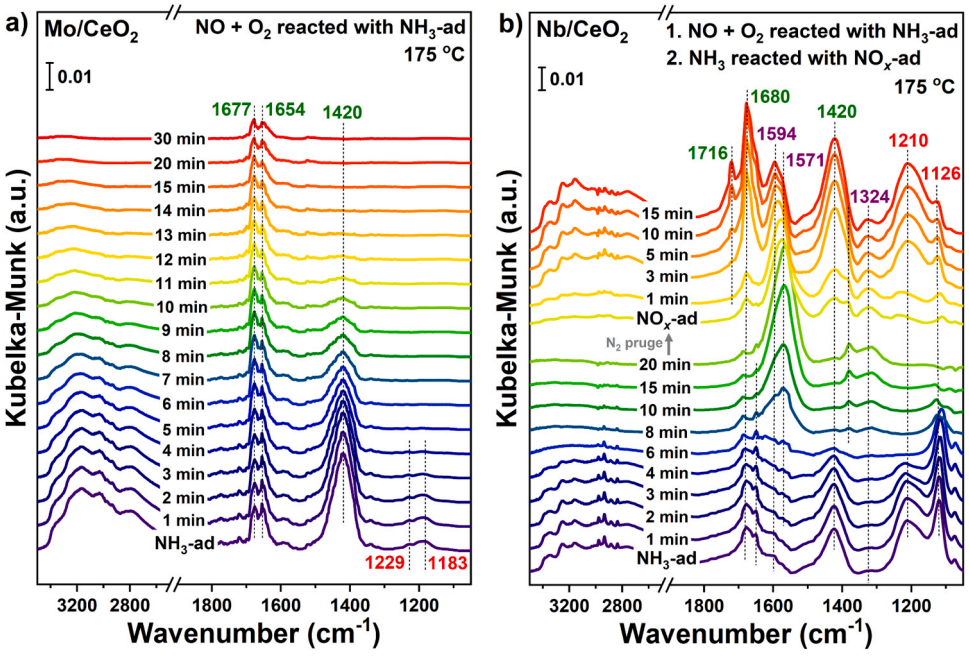

Fig. 8. **a)** *In situ* DRIFTS of NO + O_2 reacting with pre-adsorbed (NH_3-ad) NH_3 on Mo/CeO_2 catalyst. **b)** *In situ* DRIFTS of NO + O_2 reacting with NH_3-ad and NH_3 reacting with pre-adsorbed NO_x (NO_x-ad) on Nb/CeO_2 catalyst.

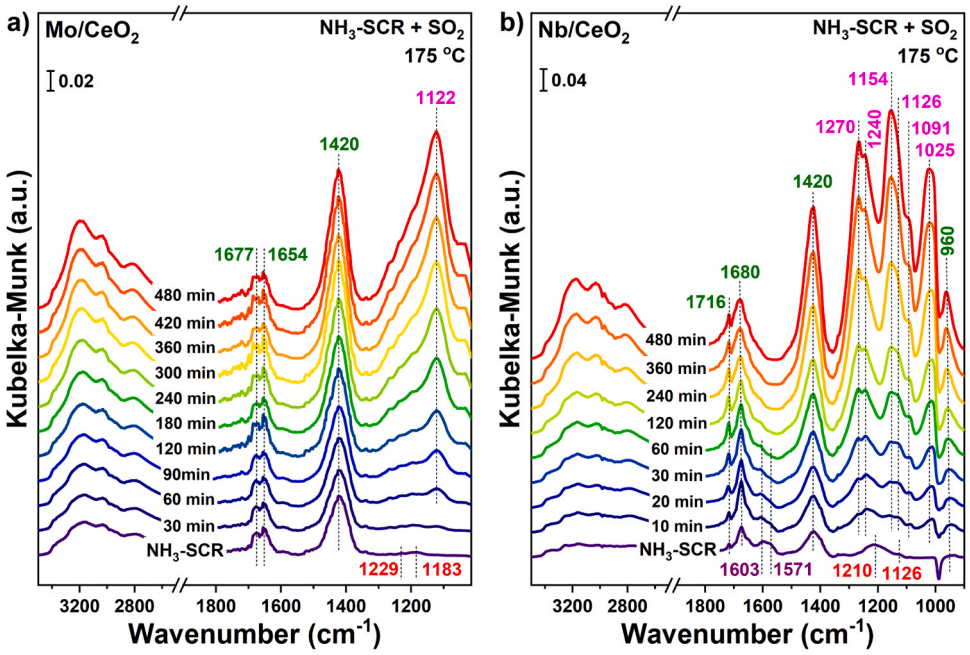

Fig. 9. *In situ* DRIFTS of NH_3-SCR + SO_2 on **a)** Mo/CeO_2 and **b)** Nb/CeO_2.

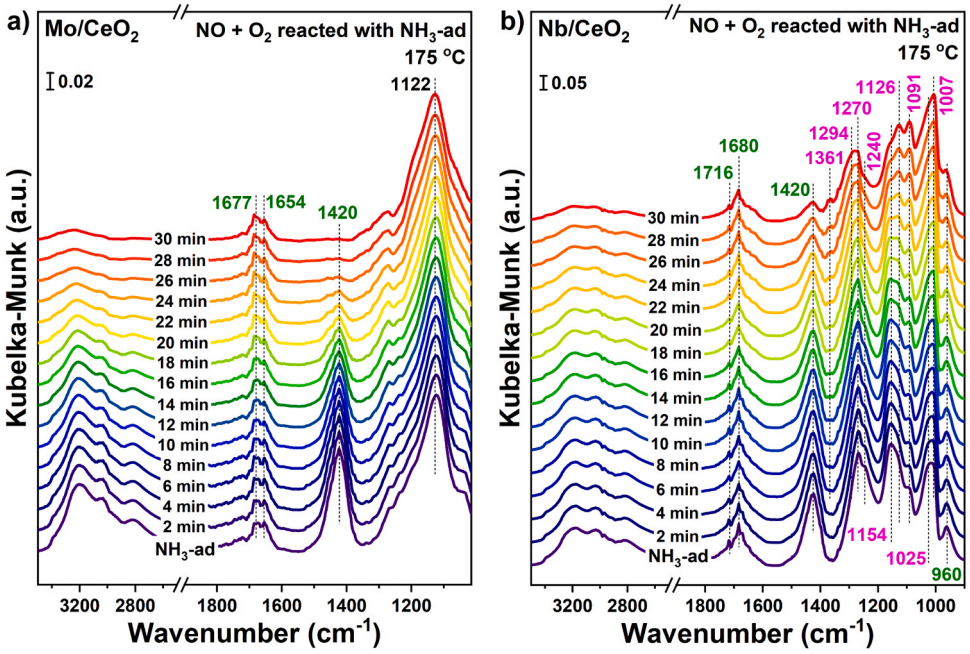

Fig. 10. *In situ* DRIFTS of NO + O_2 reacting with pre-adsorbed NH_3-ad on **a)** sulfated Mo/CeO_2 and **b)** Nb/CeO_2. The sulfation treatment was conducted as shown in Fig. 9.

3.6. Regeneration and the Role of Ammonium Sulfates

As discussed above, the deposition of ammonium sulfates or the sulfation of active sites would result in the deactivation of W/CeO_2, Mo/CeO_2 and Nb/CeO_2 catalysts. In industrial applications, calcination treatment has been widely applied for the regeneration of poisoned catalysts. Considering that ammonium sulfates deposited on W/CeO_2, Mo/CeO_2 and Nb/CeO_2 catalysts could decompose at low temperatures ($\leq$ 400 °C), W/CeO_2-used, Mo/CeO_2-used and Nb/CeO_2-used catalysts were calcined at 400 °C (lower than the calcination temperature after the impregnation of acid metal species onto CeO_2) in Ar flow for 2 h to investigate whether the removal of ammonium sulfates could help regenerate the poisoned catalysts. As shown in Fig. 11 and Fig. S9, after the regeneration treatment (400 °C, Ar flow), the NO_x conversions on W/CeO_2-used, Mo/CeO_2-used and Nb/CeO_2-used catalysts at 175 °C were all found to increase. Since SO_2 would not be released but re-captured by catalysts when ammonium sulfates decomposed, it could be concluded that ABS showed a much more significant poisoning effect on CeO_2 and CeO_2 modified with acid metal oxides than the sulfation of CeO_2. The amount of sulfate species on the regenerated catalysts was further determined by TG experiments (Fig. S10). It was found that the weight loss assigned to the decomposition of sulfate species on those regenerated catalysts was almost the same as that on corresponding used catalysts, well supporting the viewpoint that SO_2 generated by the

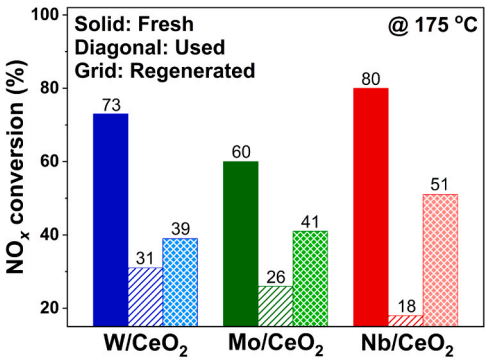

Fig. 11. NO_x conversions on fresh, used and regenerated catalysts at 175 °C.

decomposition of ammonium sulfates would be re-captured when the calcination temperature was 400 °C or lower. However, it must be noted that the calcination treatment (400 °C) might result in the deep sulfation of active sites, especially Ce species [46]. That's why the regenerated catalysts still showed poorer catalytic performance than fresh catalysts. Considering that Mo/CeO_2 showed lower reactivity to SO_2 to form sulfated CeO_2, and the deposition of ammonium sulfates was the main reason for the deactivation of Mo/CeO_2 in NH_3-SCR when exposed to SO_2, Mo-CeO_2 catalysts might show promising application perspective in some reactions in the presence of SO_2 but without NH_3.

4. Conclusion

In this work, optimal loadings of acid metal oxides (MoO_3, Nb_2O_5, WO_3) were impregnated onto CeO_2 to investigate the impact of acid metal oxide modification on CeO_2 catalyst for NH_3-SCR of NO_x. Besides the expected improvement of the activity and N_2 selectivity, significantly enhanced SO_2 resistance ability was also achieved on the CeO_2 modified with acid metal oxides comparing to bare CeO_2. Moreover, highly dispersed Mo or W species were found to better shield CeO_2 from SO_2 poisoning than highly dispersed Nb species. Besides serving as Brønsted acid sites for NH_3 adsorption/activation, highly dispersed Mo and W species could also inhibit SO_2 from directly interacting with the catalysts. It was also revealed that the consumption of highly active Lewis acid sites by SO_2 and the coverage of active sites by the deposited ammonium sulfates were the main reasons for the deactivation of CeO_2 catalysts modified with acid metal oxides. The lowest affinity of Mo/CeO_2 catalysts for SO_2 made surface Mo-O-Ce paired site an attractive element in constructing NH_3-SCR catalysts with high SO_2 resistance performance. This work provided a deep insight into designing efficient catalysts working under an SO_2-containing atmosphere.

CRediT authorship contribution statement

The manuscript was written through the contributions from all authors. All authors have given approval to the final version of the manuscript.

CRediT authorship contribution statement

Yandi Cai: Methodology, Investigation, Validation, Data curation, Writing – original draft. **Bifeng Zhang:** Methodology, Validation. **Haowei Yu:** Methodology. **Xiaoyu Ji:** Methodology. **Jingfang Sun:** Writing – review & editing. **Xizhang Wang:** Resources, Methodology. **Qiuhui Qian:** Investigation. **Lulu Li:** Writing – review & editing. **Annai Liu:** Methodology. **Wei Tan:** Supervision, Conceptualization, Investigation, Validation, Data curation, Writing – original draft, Writing – review & editing. **Fei Gao:** Supervision, Conceptualization, Writing – review & editing. **Lin Dong:** Supervision, Funding acquisition.

Declaration of Competing Interest

The authors declare that they have no known competing financial interests or personal relationships that could have appeared to influence the work reported in this paper.

Data Availability

Data will be made available on request.

Acknowledgements

The authors gratefully acknowledge the financial support from the National Natural Science Foundation of China (No. 21972063, 22272077, 22306090) and Natural Science Foundation of Jiangsu Province (BK20200012).

Appendix A. Supporting information

Supplementary data associated with this article can be found in the online version at doi:10.1016/j.apcatb.2023.123424.

References

[1] J.A. James, S. Sung, H. Jeong, O.A. Broesicke, S.P. French, D. Li, J.C. Crittenden, Impacts of combined cooling, heating and power systems, and rainwater harvesting on water demand, carbon dioxide, and NO_x emissions for atlanta, Environ. Sci. Technol. 52 (2018) 3–10.
[2] K. He, H. Huo, Q. Zhang, Urban air pollution in china: current status, characteristics, and progress, Annu. Rev. Energy Environ. 27 (2002) 397–431.
[3] M.V. Twigg, Progress and future challenges in controlling automotive exhaust gas emissions, Appl. Catal. B: Environ. 70 (2007) 2–15.
[4] R. Zhang, N. Liu, Z. Lei, B. Chen, Selective transformation of various nitrogen-containing exhaust gases toward N_2 over zeolite catalysts, Chem. Rev. 116 (2016) 3658–3721.
[5] S.M. Mousavi, H. Fatehi, X.-S. Bai, Numerical study of the combustion and application of SNCR for NO reduction in a lab-scale biomass boiler, Fuel 293 (2021).
[6] L.L. Guido Buscaa, Gianguido Ramisa, Francesco Bertic, Chemical and mechanistic aspects of the selective catalytic reduction of NO_x by ammonia over oxide catalysts: a review, Appl. Catal. B: Environ. 18 (1998) 1–36.
[7] L. Han, S. Cai, M. Gao, J.-y Hasegawa, P. Wang, J. Zhang, L. Shi, D. Zhang, Selective catalytic reduction of NO_x with NH_3 by using novel catalysts: State of the art and future prospects, Chem. Rev. 119 (2019) 10916–10976.
[8] P. Forzatti, I. Nova, E. Tronconi, A. Kustov, J.R. Thøgersen, Effect of operating variables on the enhanced SCR reaction over a commercial V_2O_5-WO_3/TiO_2 catalyst for stationary applications, Catal. Today 184 (2012) 153–159.
[9] M. Zhu, J.K. Lai, U. Tumuluri, Z. Wu, I.E. Wachs, Nature of active sites and surface intermediates during SCR of NO with NH_3 by supported V_2O_5-WO_3/TiO_2 catalysts, J. Am. Chem. Soc. 139 (2017) 15624–15627.
[10] J.L. Liang Chen, Maofa Ge, DRIFT study on cerium-tungsten titiania catalyst for selective catalytic reduction of NO_x with NH_3, Environ. Sci. Technol. 44 (2010) 9590–9596.
[11] J. Chen, Y. Chen, M. Zhou, Z. Huang, J. Gao, Z. Ma, J. Chen, X. Tang, Enhanced performance of ceria-based NO_x reduction catalysts by optimal support effect, Environ. Sci. Technol. 51 (2017) 473–478.
[12] J. Ji, Y. Tang, L. Han, P. Ran, W. Song, Y. Cai, W. Tan, J. Sun, C. Tang, L. Dong, Cerium manganese oxides coupled with ZSM-5: A novel SCR catalyst with superior K resistance, Chem. Eng. J. 445 (2022).
[13] W. Tan, J. Wang, Y. Cai, L. Li, S. Xie, F. Gao, F. Liu, L. Dong, Molybdenum oxide as an efficient promoter to enhance the NH_3-SCR performance of CeO_2-SiO_2 catalyst for NO removal, Catal. Today, 397- 399 (2022) 475–483.
[14] X. Yao, L. Chen, J. Cao, Y. Chen, M. Tian, F. Yang, J. Sun, C. Tang, L. Dong, Enhancing the deNO performance of MnO/CeO_2-ZrO_2 nanorod catalyst for low-temperature NH_3-SCR by TiO_2 modification, Chem. Eng. J. 369 (2019) 46–56.
[15] Y. Peng, K. Li, J. Li, Identification of the active sites on CeO_2-WO_3 catalysts for SCR of NO_x with NH_3: An *in situ* IR and Raman spectroscopy study, Appl. Catal. B: Environ. 140–141 (2013) 483–492.
[16] S. Ding, F. Liu, X. Shi, K. Liu, Z. Lian, L. Xie, H. He, Significant promotion effect of Mo additive on a novel Ce-Zr mixed oxide catalyst for the selective catalytic reduction of NO_x with NH_3, ACS Appl. Mater. Interfaces 7 (2015) 9497–9506.
[17] Z. Liu, H. Su, J. Li, Y. Li, Novel MoO_3/CeO_2–ZrO_2 catalyst for the selective catalytic reduction of NO_x by NH_3, Catal. Commun. 65 (2015) 51–54.
[18] S. Ding, F. Liu, X. Shi, H. He, Promotional effect of Nb additive on the activity and hydrothermal stability for the selective catalytic reduction of NO_x with NH_3 over $CeZrO_x$ catalyst, Appl. Catal. B: Environ. 180 (2016) 766–774.
[19] W. Tan, C. Wang, S. Yu, Y. Li, S. Xie, F. Gao, L. Dong, F. Liu, Revealing the effect of paired redox-acid sites on metal oxide catalysts for efficient NO_x removal by NH_3-SCR, J. Hazard. Mater. 416 (2021), 125826.

[20] L. Li, C. Ge, J. Ji, W. Tan, X. Wang, X. Wei, K. Guo, C. Tang, L. Dong, Effects of different methods of introducing Mo on denitration performance and anti-SO_2 poisoning performance of CeO_2, Chin. J. Catal. 42 (2021) 1488–1499.

[21] Y. Chen, C. Li, J. Chen, X. Tang, Self-prevention of well-defined-facet Fe_2O_3/MoO_3 against deposition of ammonium bisulfate in low-temperature NH_3-SCR, Environ. Sci. Technol. 52 (2018) 11796–11802.

[22] C. Sun, H. Liu, W. Chen, D. Chen, S. Yu, A. Liu, L. Dong, S. Feng, Insights into the Sm/Zr co-doping effects on N_2 selectivity and SO_2 resistance of a MnO_x-TiO_2 catalyst for the NH_3-SCR reaction, Chem. Eng. J. 347 (2018) 27–40.

[23] W. Tan, A. Liu, S. Xie, Y. Yan, T.E. Shaw, Y. Pu, K. Guo, L. Li, S. Yu, F. Gao, F. Liu, L. Dong, Ce-Si mixed oxide: A high sulfur resistant catalyst in the NH_3-SCR reaction through the mechanism-enhanced process, Environ. Sci. Technol. 55 (2021) 4017–4026.

[24] Y. Peng, R. Qu, X. Zhang, J. Li, The relationship between structure and activity of MoO_3-CeO_2 catalysts for NO removal: influences of acidity and reducibility, Chem. Commun. 49 (2013) 6215–6217.

[25] R. Qu, X. Gao, K. Cen, J. Li, Relationship between structure and performance of a novel cerium-niobium binary oxide catalyst for selective catalytic reduction of NO with NH_3, Appl. Catal. B: Environ. 142–143 (2013) 290–297.

[26] Z. Ma, X. Wu, H. Härelind, D. Weng, B. Wang, Z. Si, NH_3-SCR reaction mechanisms of NbO /$Ce_{0.75}Zr_{0.25}O_2$ catalyst: DRIFTS and kinetics studies, J. Mol. Catal. A: Chem. 423 (2016) 172–180.

[27] K. Guo, J. Ji, R. Osuga, Y. Zhu, J. Sun, C. Tang, J.N. Kondo, L. Dong, Construction of Fe_2O_3 loaded and mesopore confined thin-layer titania catalyst for efficient NH_3-SCR of NO_x with enhanced H_2O/SO_2 tolerance, Appl. Catal. B: Environ. 287 (2021).

[28] K. Guo, J. Ji, W. Song, J. Sun, C. Tang, L. Dong, Conquering ammonium bisulfate poison over low-temperature NH_3-SCR catalysts: A critical review, Appl. Catal. B: Environ. 297 (2021).

[29] W. Tan, J. Wang, L. Li, A. Liu, G. Song, K. Guo, Y. Luo, F. Liu, F. Gao, L. Dong, Gas phase sulfation of ceria-zirconia solid solutions for generating highly efficient and SO_2 resistant NH_3-SCR catalysts for NO removal, J. Hazard. Mater. 388 (2020), 121729.

[30] Z. Wu, M. Li, J. Howe, H.M. Meyer 3rd, S.H. Overbury, Probing defect sites on CeO_2 nanocrystals with well-defined surface planes by raman spectroscopy and O_2 adsorption, Langmuir 26 (2010) 16595–16606.

[31] S. Loridant, Raman spectroscopy as a powerful tool to characterize ceria-based catalysts, Catal. Today 373 (2021) 98–111.

[32] M. Picquart, Science and technology-structural studies during gelation of WO_3 investigated by *in-situ* raman spectroscopy, J. Sol. -Gel Sci. Technol. 18 (2000) 199–206.

[33] I.E.W. Elizabeth, I. Ross-Medgaarden, Structural determination of bulk and surface tungsten oxides with UV–vis diffuse reflectance spectroscopy and raman spectroscopy, J. Phys. Chem. C. 111 (2007) 15089–15099.

[34] X. Li, X. Li, J. Li, J. Hao, High calcium resistance of CeO_2–WO_3 SCR catalysts: Structure investigation and deactivation analysis, Chem. Eng. J. 317 (2017) 70–79.

[35] Y. Wu, G. Hu, Y. Xie, M. Guo, M. Luo, Solid state reaction of MoO_3–CeO_2 complex oxide studied by raman spectroscopy, Solid State Sci. 13 (2011) 2096–2099.

[36] W. Yu, J. Zhu, L. Qi, C. Sun, F. Gao, L. Dong, Y. Chen, Surface structure and catalytic properties of MoO_3/CeO_2 and $CuO/MoO_3/CeO_2$, J. Colloid Interface Sci. 364 (2011) 435–442.

[37] Z. Ma, X. Wu, Z. Si, D. Weng, J. Ma, T. Xu, Impacts of niobia loading on active sites and surface acidity in NbO/CeO_2–ZrO_2 NH_3–SCR catalysts, Appl. Catal. B: Environ. 179 (2015) 380–394.

[38] M.A. Bañares, I.E. Wachs, Molecular structures of supported metal oxide catalysts under different environments, J. Raman Spectrosc. 33 (2002) 359–380.

[39] J. Zhu, F. Gao, L. Dong, W. Yu, L. Qi, Z. Wang, L. Dong, Y. Chen, Studies on surface structure of $M_xO_y/MoO_3/CeO_2$ system (M = Ni, Cu, Fe) and its influence on SCR of NO by NH_3, Appl. Catal. B: Environ. 95 (2010) 144–152.

[40] H.T. Kreissl, M.M.J. Li, Y.-K. Peng, K. Nakagawa, T.J.N. Hooper, J.V. Hanna, A. Shepherd, T.-S. Wu, Y.-L. Soo, S.C.E. Tsang, Structural studies of bulk to nanosize niobium oxides with correlation to their acidity, J. Am. Chem. Soc. 139 (2017) 12670–12680.

[41] C.G. Maciel, Td.F. Silva, M.I. Hirooka, M.N. Belgacem, J.M. Assaf, Effect of nature of ceria support in CuO/CeO_2 catalyst for Prox-CO reaction, Fuel 97 (2012) 245–252.

[42] Z. Ma, D. Weng, X. Wu, Z. Si, Effects of WO_x modification on the activity, adsorption and redox properties of CeO_2 catalyst for NO_x reduction with ammonia, J. Environ. Sci. 24 (2012) 1305–1316.

[43] P.B.M. Waqif, O. Saur, J.C. Lavalley, G. Blanchard, O. Touret, Study of ceria sulfation, Appl. Catal. B: Environ. 11 (1997) 193–205.

[44] S. Yang, Y. Guo, H. Chang, L. Ma, Y. Peng, Z. Qu, N. Yan, C. Wang, J. Li, Novel effect of SO_2 on the SCR reaction over CeO_2: Mechanism and significance, Appl. Catal. B: Environ. 136–137 (2013) 19–28.

[45] J. Marlowe, S. Acharya, A. Zuber, G. Tsilomelekis, Characterization of sulfated SnO_2-ZrO_2 Catalysts and their catalytic performance on the tert-butylation of phenol, Catalysts 10 (2020).

[46] L. Zhang, W. Zou, K. Ma, Y. Cao, Y. Xiong, S. Wu, C. Tang, F. Gao, L. Dong, Sulfated temperature effects on the catalytic activity of CeO_2 in NH_3-Selective catalytic reduction conditions, J. Phys. Chem. C. 119 (2015) 1155–1163.

[47] I.N.M. Ziolek, Niobium compounds: Preparation, characterization, and application in heterogeneous catalysis, Chem. Rev. 99 (1999) 3603–3624.

[48] J.D. Loyd, J. Burcham, Israel E. Wachs, *In situ* vibrational spectroscopy studies of supported niobium oxide catalysts, J. Phys. Chem. B 103 (1999) 6015–6024.

[49] J. Zhang, Y. Fan, X. Yu, Z. Huang, W. Dai, L. Yang, Improvement on the catalytic performance of MoO_3 nanobelts for NH_3-SCR Reaction by SnO_2-modification: Enhancement of acidity and redox property, Catal. Lett. 152 (2021) 480–488.

[50] L. Kylhammar, P.-A. Carlsson, H.H. Ingelsten, H. Grönbeck, M. Skoglundh, Regenerable ceria-based SO_x traps for sulfur removal in lean exhausts, Appl. Catal. B: Environ. 84 (2008) 268–276.

[51] H.H. Wenqing Xu, Yunbo Yu, Deactivation of a $CeTiO_2$ catalyst by SO_2 in the selective catalytic reduction of NO by NH_3, J. Phys. Chem. C. 113 (2009) 4426–4432.

[52] W. Tan, Y. Cai, S. Xie, J. Xu, K. Ma, K. Ye, L. Ma, S.N. Ehrlich, W. Zou, F. Gao, L. Dong, F. Liu, Constructing efficient CuO-CeO_2 catalyst for NO reduction by CO: New insights into the structure–activity relationship, Chem. Eng. J. 456 (2023).

[53] L. Zhu, Z. Zhong, H. Yang, C. Wang, A comparative study of metal oxide and sulfate catalysts for selective catalytic reduction of NO with NH_3, Environ. Technol. 38 (2017) 1285–1294.

[54] W. Tan, J. Wang, S. Yu, A. Liu, L. Li, K. Guo, Y. Luo, S. Xie, F. Gao, F. Liu, L. Dong, Morphology-sensitive sulfation effect on ceria catalysts for NH_3-SCR, Top. Catal. 63 (2020) 932–943.

[55] Y. Xiong, C. Tang, X. Yao, L. Zhang, L. Li, X. Wang, Y. Deng, F. Gao, L. Dong, Effect of metal ions doping (M = Ti^{4+}, Sn^{4+}) on the catalytic performance of MnO/CeO_2 catalyst for low temperature selective catalytic reduction of NO with NH_3, Appl. Catal. A: Gen. 495 (2015) 206–216.

[56] F. Liu, W. Shan, Z. Lian, J. Liu, H. He, The smart surface modification of Fe_2O_3 by WO for significantly promoting the selective catalytic reduction of NO with NH_3, Appl. Catal. B: Environ. 230 (2018) 165–176.

[57] Z. Liu, S. Zhang, J. Li, L. Ma, Promoting effect of MoO_3 on the NO_x reduction by NH_3 over CeO_2/TiO_2 catalyst studied with *in situ* DRIFTS, Appl. Catal. B: Environ. 144 (2014) 90–95.

[58] L. Li, L. Zhang, K. Ma, W. Zou, Y. Cao, Y. Xiong, C. Tang, L. Dong, Ultra-low loading of copper modified TiO_2/CeO_2 catalysts for low-temperature selective catalytic reduction of NO by NH_3, Appl. Catal. B: Environ. 207 (2017) 366–375.

[59] B.J. Zhongbiao Wu, Yue Liu, Haiqiang Wang, Ruiben Jin, DRIFT study of manganese/titania-based catalysts for low-temperature selective catalytic reduction of NO with NH_3, Environ. Sci. Technol. 41 (2007) 5812–5817.

[60] X. Yao, R. Zhao, L. Chen, J. Du, C. Tao, F. Yang, L. Dong, Selective catalytic reduction of NO_x by NH_3 over CeO_2 supported on TiO_2: Comparison of anatase, brookite, and rutile, Appl. Catal. B: Environ. 208 (2017) 82–93.

[61] B. Jiang, Z. Li, S.-c Lee, Mechanism study of the promotional effect of O_2 on low-temperature SCR reaction on Fe–Mn/TiO_2 by DRIFT, Chem. Eng. J. 225 (2013) 52–58.

[62] T. Chen, B. Guan, H. Lin, L. Zhu, *In situ* DRIFTS study of the mechanism of low temperature selective catalytic reduction over manganese-iron oxides, Chin. J. Catal. 35 (2014) 294–301.

[63] J. Liu, J. Meeprasert, S. Namuangruk, K. Zha, H. Li, L. Huang, P. Maitarad, L. Shi, D. Zhang, Facet–activity relationship of TiO_2 in Fe_2O_3/TiO_2 nanocatalysts for selective catalytic reduction of NO with NH_3: *In situ* DRIFTs and DFT studies, J. Phys. Chem. C. 121 (2017) 4970–4979.